N-Port Equal/Unequal-Split Power Dividers Using Epsilon-Near-Zero Metamaterials

Ziheng Zhou, *Graduate Student Member, IEEE*, and Yue Li, *Senior Member, IEEE*

***Abstract*— In this article, a type of multiport power divider is proposed based on the concept of epsilon-near-zero (ENZ) metamaterials. An arbitrarily shaped ENZ metamaterial comprising a dielectric impurity is connected to *N* waveguides, and the incident power can be efficiently delivered to output waveguides, with transmitted fields being exactly equal in both amplitude and phase for output branches. Hence, the proposed power divider allows a balanced power allocation independent on its geometrical symmetry. This design philosophy can further be extended to generic dividers with arbitrary power division ratios by modifying the widths of the output waveguides. The experimental verification is carried out in waveguide-emulated ENZ structures. The fabricated eight-way equal-split divider is measured with an average insertion loss of 0.6 dB, a transmission amplitude imbalance of 0.7 dB, and a phase imbalance of 10°, over the 10-dB return-loss bandwidth from 5.35 to 5.56 GHz. The ten-way unequal-split divider with two different groups of outputs is also prototyped, providing a custom-designed power division ratio.**

***Index Terms*— Epsilon-near-zero (ENZ) metamaterials, photonic doping, power divider, power division ratio, waveguide.**

I. Introduction

POWER dividers/combiners [1] are basic building blocks of microwave and millimeter-wave circuitries. They are typically deployed in, for example, the beamforming networks of antenna arrays as well as the high-power-capacity balanced amplifiers and mixers [2], [3]. There has been a demand to develop multiway power dividers/combiners [4]–[15] for large-scale radar and communication systems. In previous design strategies for *N*-port balanced power dividers, architectures with high geometrical symmetry, such as the axial symmetry [9]–[15], were commonly adopted.

In this work, inspired from a low-permittivity metamaterial, i.e., epsilon-near-zero (ENZ) metamaterial [16]–[18], we propose a kind of multiport power dividers allowed to be configured with more degrees of freedom and, meanwhile, yield highly balanced outputs or even controlled power division ratios [19]–[23]. The ENZ metamaterial has drawn great interests due to its extremely small optical index, where electromagnetic (EM) wave has a stretched wavelength and a vanishing wavenumber to rectify a spatially static dynamics [18], [24]. The ENZ metamaterial has boosted a bunch of unique applications [25]–[47], such as supercoupling of power through extra thin channels [18], [25]–[28], waveguide metamaterial circuits [29]–[31], enhancement of radiation directivity [32]–[36], transformation of scattering patterns [37]–[39], geometry-frequency decoupled devices [40]–[42], and so on. To efficiently tailor the effective permeability of the ENZ metamaterial, the technique of photonic doping [48], [49] was recently proposed, where one or several subwavelength dielectric impurities, coined as "photonic dopants," are introduced in an ENZ "host," constituting a doped ENZ metamaterial. These dopants impact the macroscopic response of the whole ENZ metamaterial and are, meanwhile, allowed to be arbitrary arranged. Such a property is essentially different from that of periodical metamaterials [50], whose performances are tightly related to the lattice parameters.

Here, we investigate an ENZ metamaterial connected with *N* single-mode waveguides, which is theoretically characterized by an *N*-dimensional scattering matrix. When the permeability of ENZ metamaterial is close to zero, i.e., attaining an epsilon-and-mu-near-zero (EMNZ) state, the whole material turns out to be transparent to a normal incidence. Under this condition, we further reveal the principle for choosing the parameters of input and output waveguides to ensure the impedance matching at the input port. Importantly, due to the field homogeneity in the ENZ host, transmitted electric fields in all output waveguides shall be exactly equal in amplitude and phase. Hence, the ENZ metamaterial is inherently promising for a balanced power division.

As an exemplary design, we present an eight-way equal-spilt waveguide power divider based on an irregularly shaped ENZ metamaterial doped with a ceramic block, and the whole doped system operates at the EMNZ state. The ENZ host is effectively realized between two metallic parallel plates near the cutoff frequency of the guided-wave TE_{10} mode [51]. All the rectangular waveguides connected to the ENZ metamaterial work on the fundamental mode. Over the bandwidth from 5.35 to 5.56 GHz for the reflection amplitude lower than −10 dB, transmission coefficients for the eight ways are measured around −9.6 dB, with an amplitude imbalance of 0.7 dB and a phase imbalance of 10°. The average insertion

Manuscript received September 13, 2020; revised October 31, 2020; accepted November 18, 2020. Date of publication January 13, 2021; date of current version March 4, 2021. This work was supported in part by the National Natural Science Foundation of China under Grant 61771280, in part by the Beijing Nova Program of Science and Technology under Grant Z191100001119082, the Tsinghua University Initiative Scientific Research Program under Contract 2019Z08QCX16, and in part by the National Key Research and Development Program of China under Grant 2018YFB1801603. *(Corresponding author: Yue Li.)*

The authors are with the Department of Electronic Engineering, Tsinghua University, Beijing 100084, China, and also with the Beijing National Research Center for Information Science and Technology, Tsinghua University, Beijing 10084, China (e-mail: lyee@tsinghua.edu.cn).

Color versions of one or more figures in this article are available at https://doi.org/10.1109/TMTT.2020.3045722.

Digital Object Identifier 10.1109/TMTT.2020.3045722

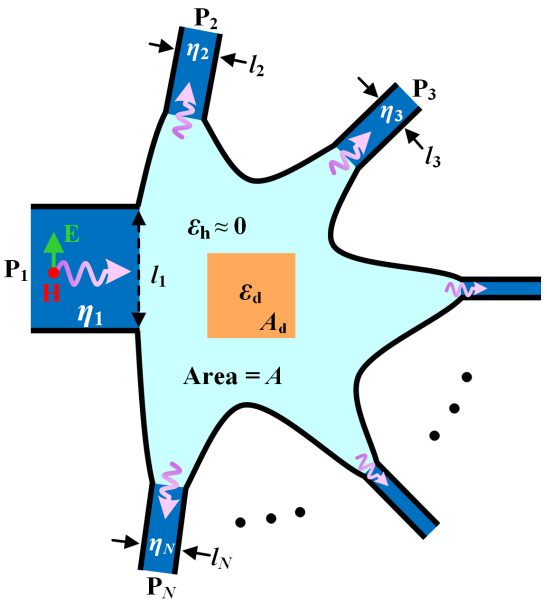

Fig. 1. Sketch of a 2-D ENZ metamaterial connected to N parallel-plate waveguides. A dielectric impurity (in orange) is embedded in the ENZ region.

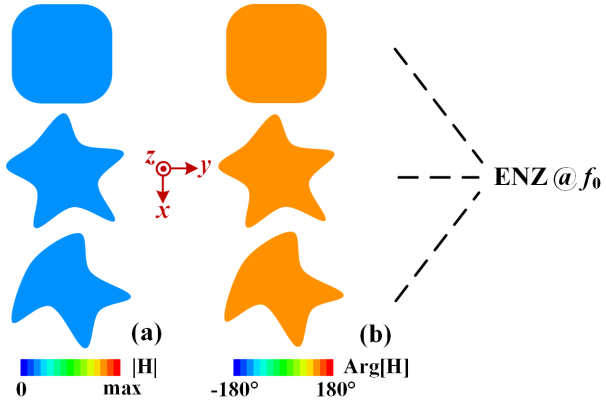

Fig. 2. Conceptual plots of the 2-D geometry-irrelevant ENZ metamaterial with uniform magnetic field (a) magnitude distribution and (b) phase distribution.

loss is tested to be 0.6 dB. By properly modifying the widths of output waveguides, our proposal can be extended to unequal-split power divider designs. For the prototyped ten-way unequal-split power divider, seven output ports are of 3 mm width and the others are of 1 mm width. Measured transmission amplitudes from the input waveguide to output waveguides of 3 mm width and 1 mm width are preserved around −9.7 dB and near −14.5 dB, respectively. Measured transmission phases for ten ways are highly consistent. Measurement results show a good agreement with the theory as well as the full-wave simulations. The salient property of the proposed power divider based on the ENZ metamaterial is to fit in irregular cross-sectional geometries.

II. Theory of N-Port ENZ Metamaterial

As conceptually sketched in Fig. 1, a 2-D arbitrarily shaped ENZ metamaterial is branched to N parallel-plate waveguides (WG_1, WG_2,…, WG_N), which are terminated by ports labeled as P_1, P_2,…, and P_N, respectively. Wave impedances of materials filling the waveguides are η_1, η_2,…, η_N.The external walls (except at the ports of waveguides) of the whole configuration are made of perfect electric conductor. Within the ENZ region, a dielectric impurity with a relative permittivity of ε_d is embedded. The total area of the ENZ metamaterial is A. The incident wave from the driven port is polarized with a magnetic field along the out-of-plane axis.

The configuration shown in Fig. 1 can be modelled by an N-port network. First, we would like to qualitatively study the wave physics underlies the geometry-irrelevance property of the ENZ metamaterial. Let us consider a 2-D ENZ metamaterial wherein the magnetic field is polarized along the out-of-plane axis. Due to the extremely low permittivity over the ENZ region, the curl of magnetic field approaches to zero [24], i.e., $\nabla \times (H\hat{z}) \approx 0$, which reduces to $\nabla H \approx 0$. Hence, as conceptually plotted in Fig. 2(a) and (b), both the magnitude and phase of magnetic field are uniformly distributed over the ENZ metamaterials at the operating frequency f_0, regardless of their detailed geometries. Such a geometry-irrelevance phenomenon, although is promising, the large wave impedance in an ENZ metamaterial is a tricky problem to tackle. A 2-D ENZ metamaterial placed in the waveguide will cause a strong reflection. To address this challenge, we apply the technique of photonic doping [48] to tailor the effective permeability of ENZ metamaterial to zero, attaining an EMNZ response, which matches the discontinuity in the waveguide configuration.

For convenience of the following derivation of the scattering matrix of the N-port ENZ metamaterial, we define in Fig. 1 the interfaces of the ENZ metamaterial with the waveguides (terminated by ports P_1, P_2,…, and P_N) as $\alpha_p (p = 1, 2,\ldots, N)$. We apply Faraday's law to yield

$$\oint_{\partial A} \mathbf{E} \cdot d\mathbf{l} = \sum_{p=1}^{N} E_p l_p = -j\omega\mu_0\mu_{\text{eff}} H_0 A \tag{1}$$

where A and A_d represent, respectively, the total area of the ENZ metamaterial and the area of dopant; E_p $(p = 1, 2,\ldots, N)$ denotes tangential electric field components on the interfaces α_p; H_0 stands for the uniformly distributed magnetic field over the ENZ host [48]; ω is the angular frequency; μ_0 is the permeability of vacuum; μ_{eff} is the effective permeability of the ENZ metamaterial [48].

We excite the network of ENZ metamaterial at an arbitrarily given port P_m and let other ports be matched. In this scenario, the electric fields $E_p (p = 1, 2,\ldots, N$ and $p \neq m)$ are actually the transmitted electric fields $E_{p,\text{out}}$ on the interfaces α_p between the ENZ host and the output waveguides WG_p, i.e., $E_p = E_{p,\text{out}}$. To derive the 2-D input impedance, which is evaluated by the electric voltage over the surface current density, (1) is reformulated as

$$-E_m l_m / H_0 = j\omega\mu_0\mu_{\text{eff}} A + \sum_{p\neq m} E_{p,\text{out}} l_p / H_0. \tag{2}$$

As seen, the left term in (2) is exactly the 2-D input impedance of the ENZ metamaterial seen at the port P_m.

Owing to the travelling wave state in the output waveguides, the transmitted electric fields $E_{p,\text{out}}$ are related to the magnetic field H_0 on the interfaces α_p, by

$$E_{p,\text{out}}/H_0 = \eta_p,\ \ p = 1, 2, .., N,\ \text{and}\ p \neq m. \tag{3}$$

Equation (3) sheds light on the fact that the scattered electric fields from the ENZ metamaterial share the same magnitude and phase, which stems from the uniform magnetic field in the ENZ host. By substituting (3) into (2), we can readily calculate the reflection coefficient seen at the driven port P_m

$$\mathbf{S}_{m,m} = \frac{-E_m l_m/H_0 - \eta_m l_m}{-E_m l_m/H_0 + \eta_m l_m} = \frac{j\omega\mu_0\mu_{\text{eff}}A + \sum_{p\neq m}\eta_p l_p - \eta_m l_m}{j\omega\mu_0\mu_{\text{eff}}A + \sum_{p\neq m}\eta_p l_p + \eta_m l_m}. \tag{4}$$

To proceed, we are going to derive the transmission coefficient from port P_m to port $P_n (n \neq m)$. Following manipulations to (2) are performed: express E_m in the left term by $(1 + \mathbf{S}_{m,m})E_{m,\text{in}}$ ($E_{m,\text{in}}$is the incident electric field on the interface α_m), and then eliminate $E_{p,\text{out}}$ on the right-hand side by using $E_{p,\text{out}} = \eta_p H_0$ (p =1, 2,..., N, $p \neq m$), and lastly, substitute $E_{n,\text{out}}/\eta_n$ for H_0 on the left-hand side. By this manner, we arrive at

$$E_{n,\text{out}}/E_{m,\text{in}} = -2\eta_n l_m \Big/ \left(j\omega\mu_0\mu_{\text{eff}}A + \sum_{p=1}^{N}\eta_p l_p \right), \quad n \neq m. \tag{5}$$

Evaluating the incident and transmitted electric voltages normalized with respect to the characteristic impedances of waveguides, we obtain the transmission coefficient

$$\begin{aligned}\mathbf{S}_{n,m} &= \frac{E_{n,\text{out}} l_n/\sqrt{\eta_n l_n}}{E_{m,\text{in}} l_m/\sqrt{\eta_m l_m}} \\ &= \frac{-2\sqrt{\eta_m\eta_n l_m l_n}}{j\omega\mu_0\mu_{\text{eff}}A + \sum_{p=1}^{N}\eta_p l_p}, \quad n \neq m.\end{aligned} \tag{6}$$

The scattering matrix of this N-port network of ENZ metamaterial can be organized in an elegant form

$$\mathbf{S}_{N\times N} = \mathbf{I}_{N\times N} - \frac{2}{j\omega\mu_0\mu_{\text{eff}}A + \sum_{p=1}^{N}\eta_p l_p}\boldsymbol{\xi}_{N\times N} \tag{7}$$

where $\mathbf{I}$ is an identity matrix, while $\boldsymbol{\xi}$ is a symmetric matrix with elements $\boldsymbol{\xi}_{n,m} = (\eta_m\eta_n l_m l_n)^{1/2}$. It should be noted that the reference planes for S-parameter calculation have been set on the interfaces of the ENZ metamaterial and waveguides. Hereafter, the port P_1 is set as the input port of the network.

Specifically, we are interested in the doped ENZ metamaterial operating at the EMNZ state, i.e., $\mu_{\text{eff}} \approx 0$. In this case, the reactance incurred by ENZ metamaterial $j\omega\mu_0\mu_{\text{eff}}A$ expressed in (4) vanishes. Therefore, the zero-reflection condition for the input port, i.e., $\mathbf{S}_{1,1} = 0$ is explicitly yielded from (4)

$$\sum_{p=2}^{N}\eta_p l_p = \eta_1 l_1. \tag{8}$$

The physical interpretation of (8) is a balance of impedances between source and loads, which are related to the parameters (widths and wave impedances) of input and output waveguides.

III. Equal-Split Power divider Design

Here, we apply the theory of the multiport ENZ metamaterial into a specific design of an $(N - 1)$-way equal-split power divider. Set: $\eta_1 l_1/(N - 1) = \eta_2 l_2 = \ldots = \eta_N l_N$, and $\mu_{\text{eff}} = 0$, the $\mathbf{S}$-matrix in (7), therefore, reduces to a straightforward form

$$\mathbf{S}_{N\times N} = \begin{bmatrix} 0 & \frac{-1}{\sqrt{N-1}} & \frac{-1}{\sqrt{N-1}} & \cdots & \frac{-1}{\sqrt{N-1}} \\ \frac{-1}{\sqrt{N-1}} & \frac{N-2}{N-1} & \frac{-1}{N-1} & \cdots & \frac{-1}{N-1} \\ \frac{-1}{\sqrt{N-1}} & \frac{-1}{N-1} & \frac{N-2}{N-1} & \ddots & \vdots \\ \vdots & \vdots & \ddots & \ddots & \frac{-1}{N-1} \\ \frac{-1}{\sqrt{N-1}} & \frac{-1}{N-1} & \cdots & \frac{-1}{N-1} & \frac{N-2}{N-1} \end{bmatrix}. \tag{9}$$

The diagonal elements signify the reflection coefficients seen at each port, where the input port P_1 has been matched ($\mathbf{S}_{1,1} = 0$). The elements in the first row/column (except for $\mathbf{S}_{1,1}$) have the same value of $-(N- 1)^{-1/2}$, manifesting in-phase equal-amplitude transmission from port P_1 to output ports P_2, P_3,..., and P_N. Other off-diagonal elements in the $\mathbf{S}$-matrix are $-1/(N- 1)$, representing coupling coefficients among output ports.

The top and 3-D perspective views of the designed eight-way waveguide power divider are presented in Fig. 3(a) and (b), respectively. The whole structure except for the ports of eight rectangular waveguides is covered by metal. The hub of the structure is constructed by an irregularly shaped air-filled waveguide with a profile $h = 27.5$ mm, which emulates the ENZ host near its cutoff frequency of TE_{10} mode, i.e., $f_0 = c/(2h) = 5.45$ GHz, where c is the speed of light in vacuum. The parameters to determine the cross-sectional geometry of the ENZ host are: $r_1 = 12.5$ mm, $r_2 = 6.25$ mm, $r_3 = 6$ mm. A dielectric block (colored in orange) with a cross-sectional area $a_d \times a_d = 14$ mm $\times$ 14 mm serves as the dopant. To suppress the coupling of TM-modes with electric field components along the z-axis, the dopant is fenced by metallic strips [48] with a width of 1 mm. The cross-sectional area A of the doped ENZ metamaterial is 670 mm^2. As labeled in the right top of Fig. 3, the dielectric constants of air, the materials filling input and output waveguides, and the dopant (ε_{air}, ε_{iw}, ε_{ow}, and ε_d) are 1, 2.1, 2.65, and 9.9, respectively. The loss tangents of the dopant material and the material filling the waveguides are 1.5×10^{-4} and 0.001, respectively. For an ideal ENZ host with a homogenous low permittivity, the position of the dopant has no impact on the macroscopic response of the doped ENZ medium. On the other hand, in the case of the realistic waveguide-emulated ENZ metamaterial, a large-size dopant close to the metallic wall can couple undesired EM modes and thus has a minor impact

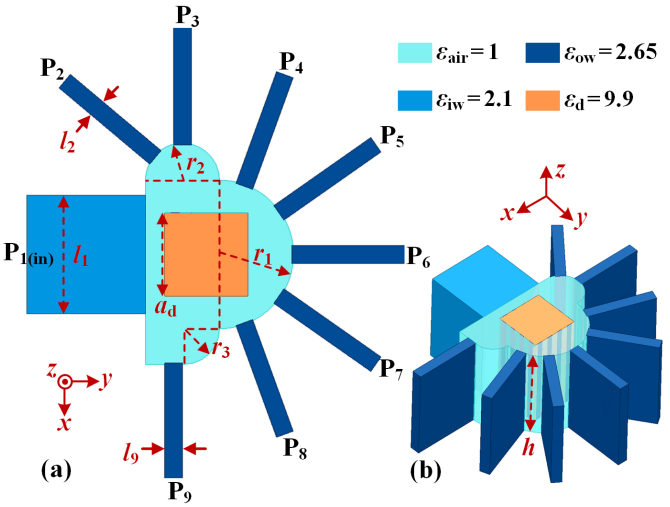

Fig. 3. (a) Top view and (b) perspective view of the proposed eight-way equal-split waveguide power divider. Dielectric constants of the materials are labeled on the right top.

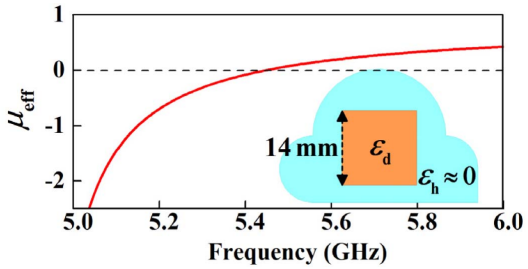

Fig. 4. Calculated relative effective permeability of the doped ENZ metamaterial, with the configuration shown in the inset.

on the consistence of the output phases. As a practical design guideline, we can locate the dopant at the geometry center of the ENZ cavity.

In [49], we have derived analytically the effective permeability of the ENZ metamaterial comprising a dopant with a square cross section

$$\mu_{\text{eff}} = 1 + \sum_{m=1,n=1}^{+\infty} \frac{4[(-1)^m - 1]^2[(-1)^n - 1]^2 a_d^2 \varepsilon_d \omega^2}{m^2 n^2 \left[c^2\pi^2(m^2+n^2)/a_d^2 - \varepsilon_d\omega^2\right]\pi^4 A}. \quad (10)$$

The calculated effective permeability for the doped ENZ medium in this design (shown in the inset of Fig. 4) is shown in Fig. 4, which crosses zero at 5.45 GHz, coincident with the cutoff frequency f_0 of the waveguide. Hence, the doped ENZ metamaterial exhibits an EMNZ response around f_0.

As for the parameters of the waveguides connected with the ENZ host, the width l_1 of the input port P_1 is 20 mm, while widths l_2, l_3…, and l_9 of output ports (P_2, P_3,…, P_9) are the same as 3 mm for the equal-split purpose. The length of input and output waveguides in Fig. 3 is all 20 mm. Taking into account the transverse resonance of the rectangular waveguide, the effective wave impedances [24], [51] near f_0 in the TE_{10}-mode driven input and output waveguides are evaluated as $(\varepsilon_{\text{iw}} - c^2/(2f_0h)^2)^{-1/2}\eta_0 = 1.1^{-1/2}\eta_0$, and $(\varepsilon_{\text{ow}} - c^2/(2f_0h)^2)^{-1/2}\eta_0 = 1.65^{-1/2}\eta_0$, respectively, where $\eta_0 = 377\ \Omega$ is the wave impedance in free space. We have checked that the condition in (8) for zero reflection power at the input port P_1 is well satisfied.

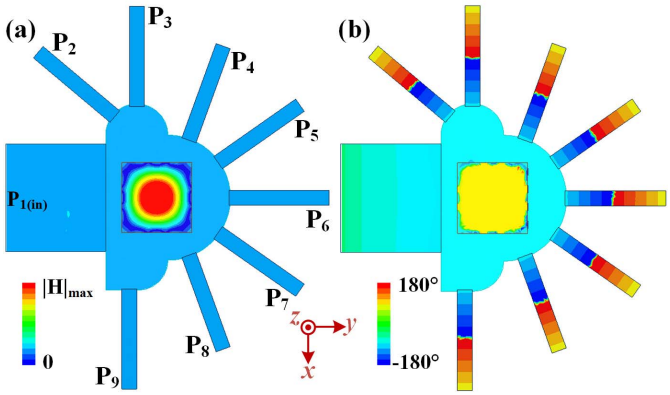

Fig. 5. Simulated (a) magnitude and (b) phase of the magnetic field H_z distributed on the middle cut plane ($z = h/2$) of the eight-way power divider at 5.45 GHz.

The full-wave simulation for the waveguide power divider is performed on the commercial software HFSS 18.0. The power divider is driven at input port P_1. Fig. 5(a) and (b) depict, respectively, the simulated magnitude and phase distribution of the z-axis-polarized magnetic field on the middle plane ($z = h/2$) at 5.45 GHz. The uniformly distributed magnetic field over the ENZ metamaterial guarantees the in-phase and equal-amplitude transmitted fields in output waveguides terminated with ports P_{2-9}. In addition, the magnetic fields in and outside the dopant are out of phase, leading to a zero net magnetic flux in the ENZ metamaterial, i.e., an effective zero permeability.

The magnitudes of simulated reflection amplitude seen at the input port P_1 and transmission amplitude for eight ways are gathered in Fig. 6(a), with an enlarged view for the transmission amplitude curves from 5.35 to 5.57 GHz. As seen, the simulated reflection amplitude $|\mathbf{S}_{1,1}|$ is lower than −10 dB from 5.35 to 5.6 GHz, around the predesigned frequency $f_0 = 5.45$ GHz due to the EMNZ response. Transmission amplitudes for eight ways ($\mathbf{S}_{2,1}$, $\mathbf{S}_{3,1}$,…, $\mathbf{S}_{9,1}$) are around −9.3 dB and maintain a maximum imbalance of 0.5 dB over the bandwidth from 5.35 to 5.57 GHz (the region colored in gray). The theoretically calculated transmission coefficients for the power divider at an idealized EMNZ state are listed in the first column/row of the $\mathbf{S}$-matrix in (9), evaluated as $20\log_{10}((N-1)^{-1/2}) = -9.03$ dB for the port number $N = 9$. The simulated transmission phases for eight ways are shown in Fig. 6(b), indicating a maximum phase imbalance of 5° over the bandwidth from 5.35 to 5.57 GHz. It shall be noted that the phase progresses in the input and output waveguides have been deembedded, so as to directly verify uniformly distributed transmission phases from the ENZ metamaterial. The coupling amplitudes among output branches $|\mathbf{S}_{m,n}|$ (m, $n = 2\ldots$, $N-1$, $m \neq n$) are also theoretically obtained from (9), being evaluated as $20\log_{10}((N-1)^{-1}) = -18.1$ dB for $N = 9$ in this design. The simulated coupling coefficients shown in Fig. 7 are consistently below −17 dB over the operating band from

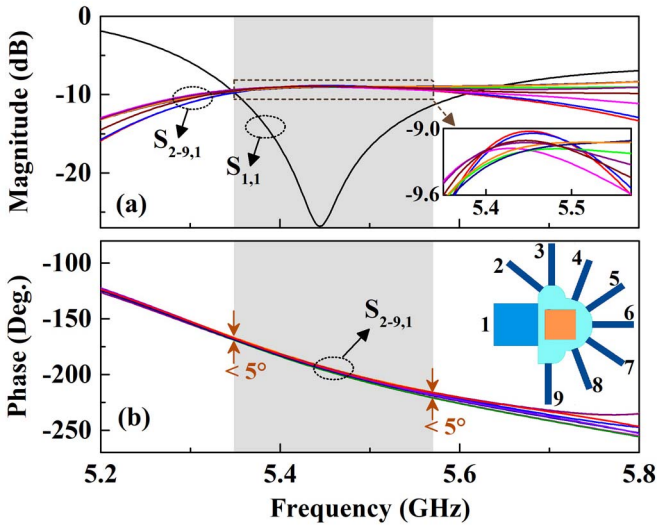

Fig. 6. (a) Simulated reflection amplitude and transmission amplitudes of the proposed eight-way equal-split power divider [shown in the inset of (b)]. (b) Simulated transmission phases.

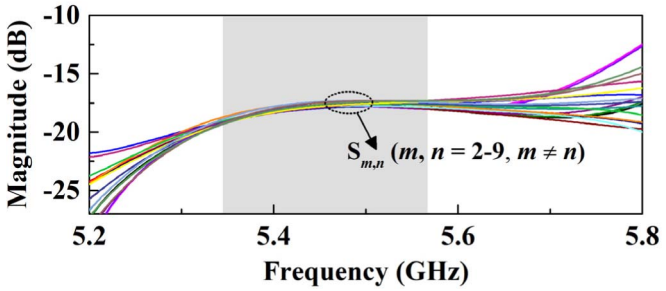

Fig. 7. Simulated mutual couplings among the output ports (P_{2-9}) of the proposed eight-way equal-split power divider.

5.35 to 5.57 GHz. In short, the eight-way power divider based on the ENZ metamaterial has been numerically verified to provide highly balanced outputs and decent isolation levels. By virtue of the large-volume dopant used in our design, the quality factor of the EMNZ resonance is reduced, which contributes to a fractional bandwidth of about 4% for the proposed metamaterial power divider.

IV. Unequal-Split Power Divider Design

In the above section, the ENZ metamaterial with a uniform magnetic field distribution has directly led to a balanced power divider. Notably, such a field homogeneity is an intrinsic feature of the ENZ metamaterial, independent on its boundary conditions, concretely, the widths and impedances of the waveguides connecting to it. We are hence allowed to modify the widths of output waveguides to attain various transmitted voltages and, furthermore, to attain various power division ratios, while will not perturb the balanced transmission phases.

The structure of prototyped ten-way unbalanced power divider is presented in Fig. 8, where Fig. 8(a) and (b) shows, respectively, the top view and 3-D perspective view. The materials and geometries for the doped ENZ metamaterial

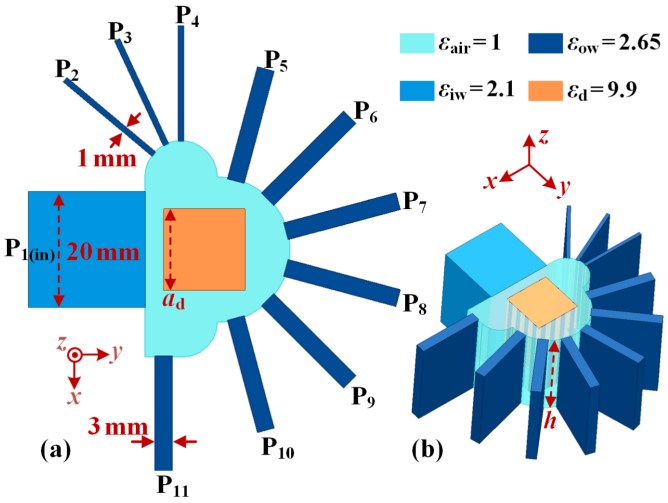

Fig. 8. (a) Top view and (b) perspective view of the proposed ten-way unequal-split waveguide power divider.

are chosen as the same as those in the previous equal-split case (Fig. 3). The EMNZ response as a result is still around $f_0 = 5.45$ GHz. Parameters of the input waveguide are set the same as that in the equal-split power divider. In this example, we custom design the power division ratio for ten ways, i.e., transmissions from P_1 to P_{2-11} as 1:1:1:3:3:3:3:3:3:3. To this end, widths of three output waveguides terminated with ports P_2, P_3, and P_4 are set as 1 mm, and seven other output waveguides terminated with P_{5-11} are all 3 mm wide. We have also checked that the condition (8) for input impedance matching at the EMNZ state is met.

As reported in Fig. 9(a), the unbalanced ten-way power divider shows a simulated impedance bandwidth for $|\mathbf{S}_{1,1}| < -10$ dB around f_0, from 5.33 to 5.58 GHz. The simulated transmission amplitudes $|\mathbf{S}_{2-4,1}|$ from input port P_1 to 1-mm output ports P_{2-4} are consistently slightly above -15 dB from 5.33 to 5.54 GHz (the region colored in gray), reaching a peak about -14.2 dB. The ideal values for $|\mathbf{S}_{2-4,1}|$ calculated by (6) are -13.8 dB. The simulated transmission amplitudes of other seven ways $|\mathbf{S}_{5-11,1}|$ are consistent around -9.4 dB, close to the ideal value of -9.03 dB calculated by (6). The difference between $|\mathbf{S}_{2-4,1}|$ and $|\mathbf{S}_{5-11,1}|$ is close to -4.77 dB over the operating band from 5.33 to 5.54 GHz, evidencing the 3:1 power division ratio (note: $10\log_{10}(3) = 4.77$ dB). The simulated transmission phases are reported in Fig. 9(b), showing a maximum phase imbalance of 5° over the operating band. As reported in Fig. 10, the simulated coupling coefficients are about -27 dB among 1-mm wide ports, -17 dB among 3-mm wide ports, and -22 dB from 1-mm wide ports to 3-mm wide ports. The theoretical coupling coefficients for these three cases are -27.6, -18.1, and -22.8 dB, respectively, calculated by (6). A good agreement has been shown between the full-wave simulation and our theoretical analysis.

V. Experimental Verifications

To validate the design philosophy of *N*-port power dividers based on the ENZ metamaterial, we fabricate and

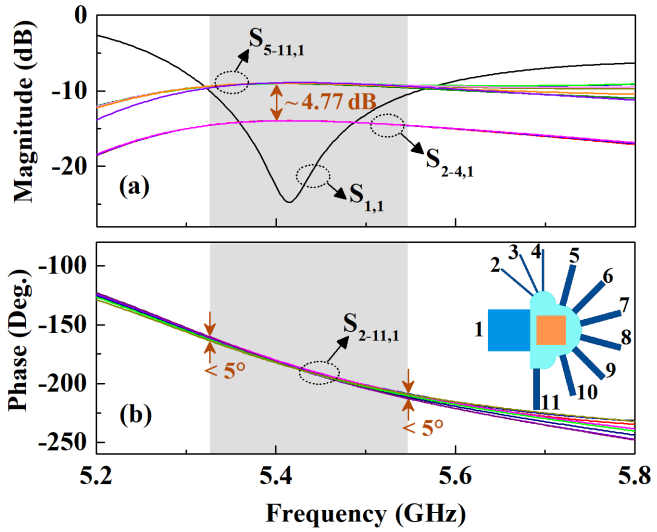

Fig. 9. (a) Simulated reflection amplitude and transmission amplitudes of the proposed ten-way unequal-split power divider [shown in the inset of (b)]. (b) Simulated transmission phases.

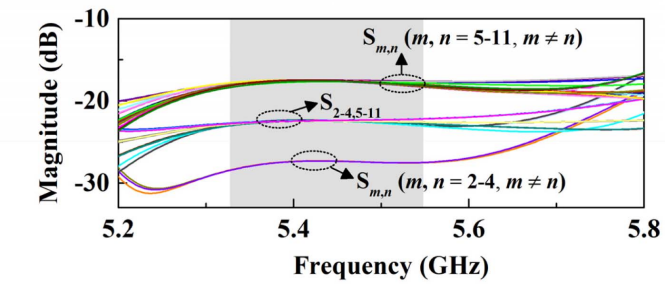

Fig. 10. Simulated mutual couplings among the output ports (P_{2-11}) of the proposed ten-way unequal-split power divider.

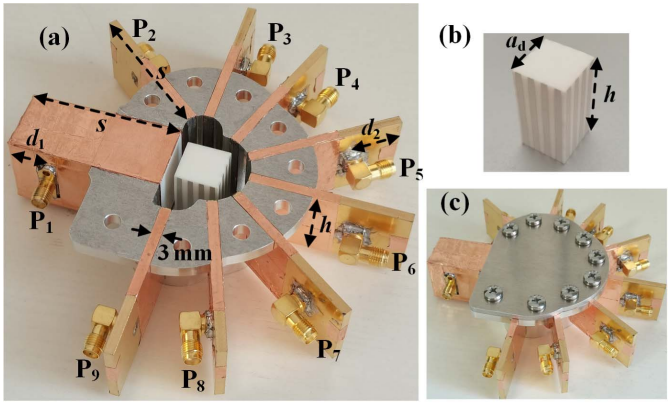

Fig. 11. (a) Photograph of the fabricated eight-way equal-split waveguide power divider (the upper metallic plate is not shown here). (b) Ceramic block fenced by metallic strips. (c) Fully assembled structure.

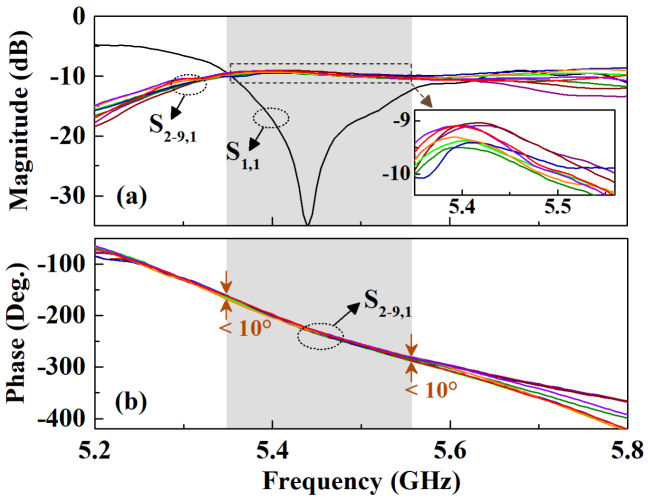

Fig. 12. (a) Measured reflection amplitude and transmission amplitudes of the fabricated eight-way equal-split divider. (b) Measured transmission phases.

experimentally characterize the prototypes of eight-way equal-split divider as well as ten-way unequal-split divider. The photograph of eight-way power divider is displayed in Fig. 11(a). The metallic cavity, with a height $h = 27.5$ mm to determine the frequency for ENZ condition, is made of solid aluminum with a conductivity of 3.8×10^7 S/m, processed via the computer-numerical-controlled (CNC) metal machining technique. The metallic flange extended from the cavity serves to clamp the waveguides in the grooves. The input waveguide connected with port P_1 is filled by Teflon with a dielectric constant of 2.1. Eight output waveguides connected with ports P_{2-9} are fabricated using the printed circuit board (PCB) technique on a 3-mm-thick substrate with a dielectric constant of 2.65 and a loss tangent ($\tan\delta$) of 0.001. Lengths of all the waveguides are $s = 50$ mm. The SMA connecters working as the input port P_1 and output ports P_{2-9} are, respectively, installed at the distances $d_1 = 11$ mm and $d_2 = 16$ mm from the endings of the corresponding waveguides. The dopant in the cavity is made of Al_2O_3 ceramic, with a dielectric constant of 9.9 and $\tan\delta = 1.5 \times 10^{-4}$. The photograph of the dopant printed with metallic strips is presented in Fig. 11(b), and the side length a_d of its cross section is 14 mm. The fully assembled structure is exhibited in Fig. 11(c).

As shown in Fig. 12(a), from 5.35 to 5.56 GHz (colored in gray), the measured reflection amplitude at the input port P_1 is below -10 dB, and transmission amplitudes for eight output branches are uniformly around -9.6 dB with a maximum imbalance of 0.7 dB. For an idealized eight-way power divider, the transmission amplitudes should be $10\log_{10}(1/8) = -9.03$ dB. Hence, the insertion loss of the prototyped power divider is as low as 0.6 dB. The measured transmission phases for eight ways are gathered in Fig. 12(b), indicating a maximum phase imbalance of 10°. The insertion loss and the phase progress in the SMA connectors have been deembedded in the calibration procedure. The measured isolation level among the output ports P_{2-9} is better than 17 dB over the operating band, as reported in Fig. 13. Overall, in agreement with the full-wave simulation as well as the theoretical analysis, the fabricated power divider based on doped ENZ metamaterial is experimentally validated to provide a low insertion loss, high balance among output ports, and descend isolation levels.

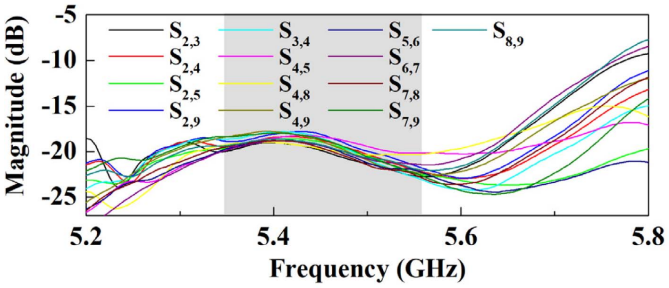

Fig. 13. Measured mutual couplings among the output ports (P_{2-9}) of the fabricated eight-way equal-split power divider.

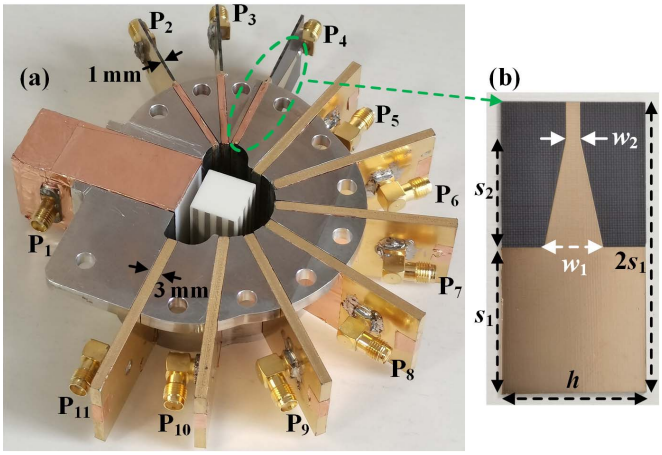

Fig. 14. (a) Photograph of the fabricated ten-way unequal-split waveguide power divider (the upper metallic plate is not shown here). (b) Waveguide-to-microstrip transition.

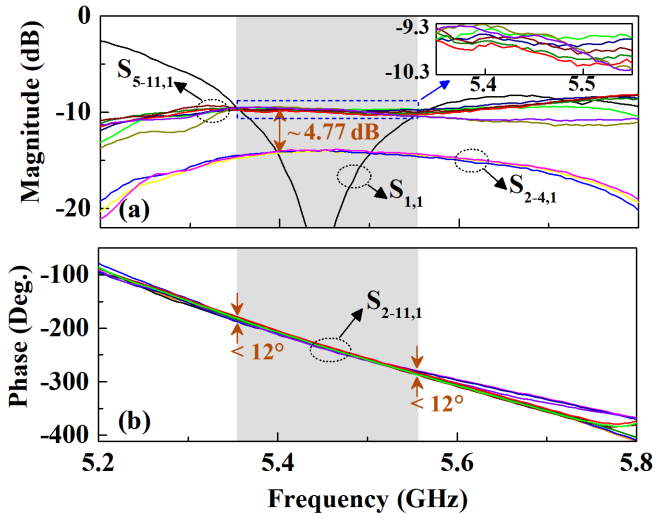

Fig. 15. (a) Measured reflection amplitude and transmission amplitudes of the fabricated ten-way unequal-split power divider. (b) Measured transmission phases.

The photograph of the prototyped unequal-split ten-way divider is presented in Fig. 14(a). The techniques and materials to fabricate the cavities and the waveguides are the same as those used in equal-split divider in Fig. 11(a). The parameters

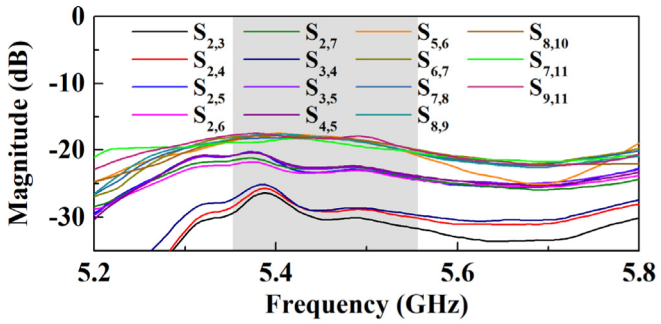

Fig. 16. Measured mutual couplings among the output ports (P_{2-11}) of the fabricated ten-way unequal-split power divider.

of the ceramic block and the air-filled cavity also follow the previous example. It is noted that there are two groups of output ports: P_{2-4} installed on 1-mm-thick waveguides and P_{5-11} on 3-mm-thick waveguides. The transition of the 1-mm-thick waveguide to the 50-Ω microstrip line is shown in Fig. 14(b), with geometry parameters given by $h = 27.5$ mm, $w_1 = 11$ mm, $w_2 = 2.7$ mm, $s_1 = 27$ mm, and $s_2 = 20$ mm. The waveguide-to-microstrip-line transition is a convenient choice to efficiently couple the power from an extremely low-profile waveguide.

As shown in Fig. 15(a), over the bandwidth from 5.36 to 5.56 GHz for $|\mathbf{S}_{1,1}| < -10$ dB, the measured transmission amplitudes from input port P_1 to P_{2-4} are around −14.5 dB, while transmission amplitudes from port P_1 to ports P_{5-11} are consistently around −9.7 dB. The difference between those two groups of transmission amplitudes approaches to 4.77 dB (note: $10\log_{10}(3) = 4.77$ dB), evidencing a power division ratio near 3:1 between any one 3-mm wide and any one 1-mm wide output waveguide. The measured transmission phases for all ten ways in Fig. 15(b) show a high consistence, with a maximum phase imbalance of 12°. To increase the power levels of output signals, the waveguide power amplifier [52], [53] can be further implemented in the input waveguide. Representative results for the measured coupling amplitudes among the output ports P_{2-11} are presented in Fig. 16, where three bunches of curves are observed in agreement with the simulation counterpart (Fig. 10). The isolation level for the worst case is better than 17.5 dB. As a result, the power divider based on the ENZ metamaterial can satisfy the necessity of the in-phase power division with custom-designed unbalanced amplitude distributions.

VI. Conclusion

In summary, inspired by an ENZ metamaterial, we propose a class of power dividers with relaxed requirement of high geometrical symmetry for balanced outputs. The ENZ metamaterial with an extreme low wave number suppresses the spatial variation of the EM fields and provides the magnetic field homogeneity. Hence, the scattered fields from the ENZ metamaterial to all output ports are equal in phase and amplitude. Furthermore, we employ a dielectric impurity to engineer the ENZ metamaterial to be matched. In proof-of-concept demonstrations, the prototyped eight-way equal-split

waveguide power divider is measured to offer a low insertion loss of 0.6 dB, an output amplitude imbalance of only 0.7 dB, and a phase imbalance of 10°, over the operating band from 5.35 to 5.56 GHz. The ten-way asymmetry power divider is experimentally characterized to provide a custom-designed power division ratio of 1:1:1:3:3:3:3:3:3:3 and highly uniform transmission phases. Our design is envisioned to provide more degrees of freedom for power dividing and combining architectures in future microwave/millimeter-wave circuits.

REFERENCES

[1] D. M. Pozar, *Microwave Engineering*, 3rd ed. New York, NY, USA: Wiley, 2005.

[2] K. J. Russell, "Microwave power combining techniques," *IEEE Trans. Microw. Theory Techn.*, vol. MTT-27, no. 5, pp. 472–478, May 1979.

[3] K. Chang and C. Sun, "Millimeter-wave power-combining techniques," *IEEE Trans. Microw. Theory Techn.*, vol. MTT-31, no. 2, pp. 91–107, Feb. 1983.

[4] M. Nakatsugawa and K. Nishikawa, "A novel configuration for 1:N multiport power dividers using series/parallel transmission-line division and a polyimide/alumina-ceramic structure for HPA module implementation," *IEEE Trans. Microw. Theory Techn.*, vol. 49, no. 6, pp. 1187–1193, Jun. 2001.

[5] J. Pollak *et al.*, "Compact waveguide-based power divider feeding independently any number of coaxial lines," *IEEE Trans. Microw. Theory Techn.*, vol. 55, no. 5, pp. 951–957, May 2007.

[6] Q.-X. Chu, Z.-Y. Kang, Q.-S. Wu, and D.-Y. Mo, "An in-phase output Ka-band traveling-wave power divider/combiner using double ridge-waveguide couplers," *IEEE Trans. Microw. Theory Techn.*, vol. 61, no. 9, pp. 3247–3253, Sep. 2013.

[7] L. W. Epp, D. J. Hoppe, A. R. Khan, and S. L. Stride, "A high-power *Ka*-band (31–36 GHz) solid-state amplifier based on low-loss corporate waveguide combining," *IEEE Trans. Microw. Theory Techn.*, vol. 56, no. 8, pp. 1899–1908, Aug. 2008.

[8] D.-S. Eom, J. Byun, and H.-Y. Lee, "Multilayer substrate integrated waveguide four-way out-of-phase power divider," *IEEE Trans. Microw. Theory Techn.*, vol. 57, no. 12, pp. 3469–3476, Dec. 2009.

[9] D. I. L. de Villiers, P. W. van der Walt, and P. Meyer, "Design of conical transmission line power combiners using tapered line matching sections," *IEEE Trans. Microw. Theory Techn.*, vol. 56, no. 6, pp. 1478–1484, Jun. 2008.

[10] K. Song, Y. Fan, and Y. Zhang, "Eight-way substrate integrated waveguide power divider with low insertion loss," *IEEE Trans. Microw. Theory Techn.*, vol. 56, no. 6, pp. 1473–1477, Jun. 2008.

[11] K. Song and Q. Xue, "Planar probe coaxial-waveguide power combiner/divider," *IEEE Trans. Microw. Theory Techn.*, vol. 57, no. 11, pp. 2761–2767, Nov. 2009.

[12] Q. Chu, D. Mo, and Q. Wu, "An isolated radial power divider via circular waveguide TE_{10}-mode transducer," *IEEE Trans. Microw. Theory Techn.*, vol. 63, no. 12, pp. 3988–3996, Dec. 2015.

[13] M. H. Chen, "A 19-way isolated power divider via the TE_{01} circular waveguide mode transition," in *IEEE MTT-S Int. Microw. Symp. Dig.*, Jun. 1986, pp. 511–513.

[14] T.-I. Hsu and M. D. Simonutti, "A wideband 60 GHz 16-way power divider/combiner network," in *IEEE MTT-S Int. Microw. Symp. Dig.*, May 1984, pp. 175–177.

[15] A. E. Fathy, S.-W. Lee, and D. Kalokitis, "A simplified design approach for radial power combiners," *IEEE Trans. Microw. Theory Techn.*, vol. 54, no. 1, pp. 247–255, Jan. 2006.

[16] S. Enoch, G. Tayeb, P. Sabouroux, N. Guérin, and P. Vincent, "A metamaterial for directive emission," *Phys. Rev. Lett.*, vol. 89, no. 21, Nov. 2002, Art. no. 213902.

[17] R. W. Ziolkowski, "Propagation in and scattering from a matched metamaterial having a zero index of refraction," *Phys. Rev. E, Stat. Phys. Plasmas Fluids Relat. Interdiscip. Top.*, vol. 70, no. 4, Oct. 2004, Art. no. 046608.

[18] M. Silveirinha and N. Engheta, "Tunneling of electromagnetic energy through subwavelength channels and bends using ε-near-zero materials," *Phys. Rev. Lett.*, vol. 97, no. 15, Oct. 2006, Art. no. 157403.

[19] T. Qi, S. He, Z. Dai, and W. Shi, "Novel unequal dividing power divider with 50 Ω characteristic impedance lines," *IEEE Microw. Wireless Compon. Lett.*, vol. 26, no. 3, pp. 180–182, Mar. 2016.

[20] K.-K.-M. Cheng and P.-W. Li, "A novel power-divider design with unequal power-dividing ratio and simple layout," *IEEE Trans. Microw. Theory Techn.*, vol. 57, no. 6, pp. 1589–1594, Jun. 2009.

[21] X. Wang, K.-L. Wu, and W.-Y. Yin, "A compact gysel power divider with unequal power-dividing ratio using one resistor," *IEEE Trans. Microw. Theory Techn.*, vol. 62, no. 7, pp. 1480–1486, Jul. 2014.

[22] B. Li, X. Wu, and W. Wu, "A 10:1 unequal wilkinson power divider using coupled lines with two shorts," *IEEE Microw. Wireless Compon. Lett.*, vol. 19, no. 12, pp. 789–791, Dec. 2009.

[23] T. Zhang, W. Che, and H. Chen, "Miniaturized multiway unequal power divider with controllable characteristic impedances," *IEEE Microw. Wireless Compon. Lett.*, vol. 27, no. 12, pp. 1062–1064, Dec. 2017.

[24] A. M. Mahmoud and N. Engheta, "Wave–matter interactions in epsilon-and-mu-near-zero structures," *Nature Commun.*, vol. 5, no. 1, pp. 1–7, Dec. 2014.

[25] M. Mitrovic, B. Jokanovic, and N. Vojnovic, "Wideband tuning of the tunneling frequency in a narrowed epsilon-near-zero channel," *IEEE Antennas Wireless Propag. Lett.*, vol. 12, pp. 631–634, 2013.

[26] N. Vojnovic, B. Jokanovic, M. Radovanovic, F. Medina, and F. Mesa, "Modeling of nonresonant longitudinal and inclined slots for resonance tuning in ENZ waveguide structures," *IEEE Trans. Antennas Propag.*, vol. 63, no. 11, pp. 5107–5113, Nov. 2015.

[27] Y. Li and N. Engheta, "Supercoupling of surface waves with ε-near-zero metastructures," *Phys. Rev. B, Condens. Matter*, vol. 90, no. 20, Nov. 2014, Art. no. 201107.

[28] Y. He *et al.*, "Wideband epsilon-near-zero supercoupling control through substrate-integrated impedance surface," *Adv. Theory Simul.*, vol. 2, no. 8, May 2019, Art. no. 1900059.

[29] Y. Li, I. Liberal, C. Della Giovampaola, and N. Engheta, "Waveguide metatronics: Lumped circuitry based on structural dispersion," *Sci. Adv.*, vol. 2, no. 6, Jun. 2016, Art. no. e1501790.

[30] Z. Zhou *et al.*, "General impedance matching via doped epsilon-near-zero media," *Phys. Rev. A, Gen. Phys.*, vol. 13, no. 3, Mar. 2020, Art. no. 034005.

[31] Y. Li, I. Liberal, and N. Engheta, "Structural dispersion–based reduction of loss in epsilon-near-zero and surface plasmon polariton waves," *Sci. Adv.*, vol. 5, no. 10, Oct. 2019, Art. no. eaav3764.

[32] M. Navarro-Cía, M. Beruete, I. Campillo, and M. Sorolla, "Enhanced lens by ε and μ near-zero metamaterial boosted by extraordinary optical transmission," *Phys. Rev. B, Condens. Matter*, vol. 83, no. 11, Mar. 2011, Art. no. 115112.

[33] D. Li, Z. Szabo, X. Qing, E.-P. Li, and Z. N. Chen, "A high gain antenna with an optimized metamaterial inspired superstrate," *IEEE Trans. Antennas Propag.*, vol. 60, no. 12, pp. 6018–6023, Dec. 2012.

[34] V. Pacheco-Peña *et al.*, "Mechanical 144 GHz beam steering with all-metallic epsilon-near-zero lens antenna," *Appl. Phys. Lett.*, vol. 105, no. 24, Dec. 2014, Art. no. 243503.

[35] D. Mitra, A. Sarkhel, O. Kundu, and S. R. B. Chaudhuri, "Design of compact and high directive slot antennas using grounded metamaterial slab," *IEEE Antennas Wireless Propag. Lett.*, vol. 14, pp. 811–814, 2015.

[36] E. Forati, G. W. Hanson, and D. F. Sievenpiper, "An epsilon-near-zero total-internal-reflection metamaterial antenna," *IEEE Trans. Antennas Propag.*, vol. 63, no. 5, pp. 1909–1916, May 2015.

[37] V. Torres *et al.*, "Experimental demonstration of a millimeter-wave metallic ENZ lens based on the energy squeezing principle," *IEEE Trans. Antennas Propag.*, vol. 63, no. 1, pp. 231–239, Jan. 2015.

[38] J. C. Soric and A. Alu, "Longitudinally independent matching and arbitrary wave patterning using ε-near-zero channels," *IEEE Trans. Microw. Theory Techn.*, vol. 63, no. 11, pp. 3558–3567, Nov. 2015.

[39] L. Zhao, Y. Feng, B. Zhu, and J. Zhao, "Electromagnetic properties of magnetic epsilon-near-zero medium with dielectric dopants," *Opt. Exp.*, vol. 27, no. 14, pp. 20073–20083, Jul. 2019.

[40] I. Liberal, A. M. Mahmoud, and N. Engheta, "Geometry-invariant resonant cavities," *Nature Commun.*, vol. 7, no. 1, Mar. 2016, Art. no. 10989.

[41] Z. Zhou and Y. Li, "Effective epsilon-near-zero (ENZ) antenna based on transverse cutoff mode," *IEEE Trans. Antennas Propag.*, vol. 67, no. 4, pp. 2289–2297, Apr. 2019.

[42] Z. Zhou and Y. Li, "A photonic-doping-inspired SIW antenna with length-invariant operating frequency," *IEEE Trans. Antennas Propag.*, vol. 68, no. 7, pp. 5151–5158, Jul. 2020.

[43] J. C. Soric, N. Engheta, S. Maci, and A. Alu, "Omnidirectional metamaterial antennas based on ε-near-zero channel matching," *IEEE Trans. Antennas Propag.*, vol. 61, no. 1, pp. 33–44, Jan. 2013.

[44] S. S. M. Khaleghi, G. Moradi, R. S. Shirazi, and A. Jafargholi, "Microstrip line impedance matching using ENZ metamaterials, design, and application," *IEEE Trans. Antennas Propag.*, vol. 67, no. 4, pp. 2243–2251, Apr. 2019.
[45] E. Baladi and A. K. Iyer, "Far-field magnification of subdiffraction conducting features using metamaterial-lined aperture arrays," *IEEE Trans. Antennas Propag.*, vol. 66, no. 7, pp. 3482–3490, Jul. 2018.
[46] J. Xiong, X. Lin, Y. Yu, M. Tang, S. Xiao, and B. Wang, "Novel flexible dual-frequency broadside radiating rectangular patch antennas based on complementary planar ENZ or MNZ metamaterials," *IEEE Trans. Antennas Propag.*, vol. 60, no. 8, pp. 3958–3961, Aug. 2012.
[47] I. Liberal and N. Engheta, "Multiqubit subradiant states in N-port waveguide devices: ε-and-μ-near-zero hubs and nonreciprocal circulators," *Phys. Rev. A, Gen. Phys.*, vol. 97, no. 2, Feb. 2018, Art. no. 022309.
[48] I. Liberal, A. M. Mahmoud, Y. Li, B. Edwards, and N. Engheta, "Photonic doping of epsilon-near-zero media," *Science*, vol. 355, no. 6329, pp. 1058–1062, Mar. 2017.
[49] Z. Zhou, Y. Li, H. Li, W. Sun, I. Liberal, and N. Engheta, "Substrate-integrated photonic doping for near-zero-index devices," *Nature Commun.*, vol. 10, no. 1, pp. 1–8, Sep. 2019.
[50] T. J. Cui, D. R. Smith, and R. Liu, *Metamaterials: Theory, Design, and Applications*. New York, NY, USA: Springer, 2009.
[51] W. Rotman, "Plasma simulation by artificial dielectrics and parallel-plate media," *IRE Trans. Antennas Propag.*, vol. 10, no. 1, pp. 82–95, Jan. 1962.
[52] M. Abdolhamidi and M. Shahabadi, "X-band substrate integrated waveguide amplifier," *IEEE Microw. Wireless Compon. Lett.*, vol. 18, no. 12, pp. 815–817, Dec. 2008.
[53] U. K. Chettiar and N. Engheta, "Metatronic transistor amplifier," *Phys. Rev. B, Condens. Matter*, vol. 92, no. 16, Oct. 2015, Art. no. 165413.

Ziheng Zhou (Graduate Student Member, IEEE) received the B.S. degree in physics from Nanjing University, Nanjing, China, in 2017. He is currently pursuing the Ph.D. degree in electronic engineering at Tsinghua University, Beijing, China.

His research interests include index-near-zero metamaterials, metasurfaces, metamaterial circuitries, electromagnetic absorbers, electromagnetic sensors, circularly polarized antennas, and metamaterial-assisted antennas.

Mr. Zhou was a recipient of the Best Student letter Awards from the conference IEEE ISAP 2019. He is serving as a Reviewer of the IEEE TRANSACTIONS ON ANTENNAS AND PROPAGATION and the IEEE ANTENNAS AND WIRELESS PROPAGATION LETTERS.

Yue Li (Senior Member, IEEE) received the B.S. degree in telecommunication engineering from Zhejiang University, Zhejiang, China, in 2007, and the Ph.D. degree in electronic engineering from Tsinghua University, Beijing, China, in 2012.

In June 2012, he joined the Department of Electronic Engineering, Tsinghua University, as a Post-Doctoral Fellow. In December 2013, he joined the Department of Electrical and Systems Engineering, University of Pennsylvania, Philadelphia, PA, USA, as a Research Scholar. He was also a Visiting Scholar with the Institute for Infocomm Research (I2 R), A∗STAR, Singapore, in 2010, and the Hawaii Center of Advanced Communication (HCAC), University of Hawaii at Manoa, Honolulu, HI, USA, in 2012. Since January 2016, he has been with Tsinghua University, where he is an Assistant Professor. He is currently an Associate Professor with the Department of Electronic Engineering, Tsinghua University. He has authored or coauthored over 150 journal articles and 45 international conference articles, and holds 20 granted Chinese patents. His current research interests include metamaterials, plasmonics, electromagnetics, nanocircuits, mobile and handset antennas, MIMO and diversity antennas, and millimeter-wave antennas and arrays.

Dr. Li was a recipient of the Issac Koga Gold Medal from URSI General Assembly in 2017; the Second Prize of Science and Technology Award of China Institute of Communications in 2017; the Young Scientist Awards from the conferences of PIERS 2019, ACES 2018, AT-RASC 2018, AP-RASC 2016, EMTS 2016, and URSI GASS 2014; the Best letter Awards from the conferences of APCAP 2020/2017, UCMMT 2020, ISAP 2019, CSQRWC 2018, NCMMW 2018/2017, NCANT 2019/2017, ISAPE 2016, and ICMMT 2020/2016; the Outstanding Doctoral Dissertation of Beijing Municipality in 2013, and the Principal Scholarship of Tsinghua University in 2011. He is serving as the Associate Editor of the IEEE TRANSACTIONS ON ANTENNAS AND PROPAGATION, the IEEE ANTENNAS AND WIRELESS PROPAGATION LETTERS, MICROWAVE AND OPTICAL TECHNOLOGY LETTERS, and the *Computer Applications in Engineering Education*, and also as the Editorial Board of Scientific Report.